Expression of ALS-linked SOD1 mutation in motoneurons or myotubes induces differential effects on neuromuscular function *in vitro*

Salim Benlefki[1#], Ana Sanchez-Vicente[1#], Vanessa Milla[1#], Olivier Lucas[1], Claire Soulard[1], Richard Younes[1,4], Csilla Gergely[2], Mélissa Bowerman[1,3], Cédric Raoul[1], Frédérique Scamps[1$*], Cécile Hilaire[1$*]

[1] The Neuroscience Institute of Montpellier, Inserm UMR1051, Univ Montpellier, Saint Eloi Hospital, Montpellier, France

[2] Charles Coulomb laboratory, L2C, UMR5221, Montpellier University, CNRS, Montpellier, France

[3] Present address. School of Medicine, Keele University, Staffordshire, UK and; Institute for Science and Technology in Medicine, Stoke-on-Trent, UK and; Wolfson Centre for Inherited Neuromuscular Disease, RJAH Orthopaedic Hospital, Oswestry, UK

[4] Neuroscience Research Center, Faculty of Medical Sciences, Lebanese University, Beirut, Lebanon

contribute equally

$ contribute equally

*corresponding author. E-mail: frederique.scamps@inserm.fr; cecile.hilaire@umontpellier.fr

Abstract

Amyotrophic lateral sclerosis (ALS) is a fatal neurodegenerative disease that selectively affects upper and lower motoneurons. Dismantlement of the neuromuscular junction (NMJ) is an early pathological hallmark of the disease whose cellular origin remains still debated. We developed an *in vitro* NMJ model to investigate the differential contribution of motoneurons and muscle cells expressing ALS-causing mutation in the superoxide dismutase 1 (SOD1) to neuromuscular dysfunction. The primary co-culture system allows the formation of functional NMJs and fosters the expression of the ALS-sensitive fast fatigable type II-b myosin heavy chain isoform. Expression of $SOD1^{G93A}$ in myotubes does not prevent the formation of a functional NMJ but leads to decreased contraction frequency and lowers the slow type I myosin heavy chain isoform transcript level. Expression of $SOD1^{G93A}$ in both motoneurons and myotubes or in motoneurons alone however alters the formation of a functional NMJ. Our results strongly suggest that diseased motoneurons are a major factor involved in the process of NMJ dismantlement in an experimental model of ALS.

Keywords

amyotrophic lateral sclerosis, myotube contraction, electrical activity, mouse primary cell culture, neuromuscular junction

Highlights

- Myotubes expressing the ALS-causing SOD1 mutant show reduced contraction frequency
- The presence of mutated SOD1 in myotube leads to reduced levels of the slow myosin heavy chain isoform
- Expression of *$SOD1^{G93A}$* in motoneurons impairs the formation of functional neuromuscular junctions

INTRODUCTION

ALS is a fatal neurodegenerative disease characterized by early denervation of the NMJ and death of motoneurons leading to progressive muscular paralysis. It is now demonstrated that motoneuron degeneration is not an exclusive cell-autonomous process but involves different cell types (Taylor et al., 2016). Skeletal muscle is the main target of motoneurons and a major player in motoneuron survival and synaptogenesis during development (Oppenheim, 1989). Mice overexpressing ALS-associated mutated human SOD1 specifically in skeletal muscles develop progressive muscle atrophy with mitochondrial dysfunction (Dobrowolny et al., 2008, Wong and Martin, 2010). Such alterations that impact skeletal muscle metabolism can induce NMJ instability, a contributing factor to muscle weakness and motoneuron degeneration (Dupuis et al., 2009, Loeffler et al., 2016). It was thus proposed that skeletal muscle is a causal factor of ALS pathology. However, it was subsequently shown that improving muscle metabolism is not sufficient to extent survival of ALS mice suggesting that skeletal muscle does not actually influence motoneuron survival in this neurodegenerative disease (Da Cruz et al., 2012). In addition, the RNA interference-mediated reduction of SOD1 mutant in skeletal muscle does not alter the course of the disease in mice (Towne et al., 2008). More recently, it was proposed that muscle-secreted factors might contribute to NMJ destabilization and axon degeneration (Maimon et al., 2018).

In addition to the role of muscle metabolism in ALS progression, the contribution of satellite cells to muscle dysfunction has also drawn attention. Indeed, muscle undergoes continuous fiber renewal throughout our life course and following injury. This process is ensured by resident satellite cells. These myogenic precursors are responsible for muscle formation, are activated during regeneration following muscle injury and play a key role in the maintenance of muscle mass (Charge and Rudnicki, 2004). Degenerative conditions, including aging and defects in satellite cell regulation, can impair muscle regeneration (Dumont et al., 2015). Abnormalities of satellite cells and repair capacity have also been observed in ALS patients (Pradat et al., 2011) and in a mouse model of the disease (Manzano et al., 2013), suggesting a loss in their muscle renewal ability that could contribute to muscle atrophy in ALS.

Little is known regarding the independent contribution of muscle and motoneuron for NMJ formation and dismantling in ALS. To address their specific roles under pathological conditions, we set-up an *in vitro* model which allows assessing the potential of satellite cells to differentiate into myotubes and make a functional NMJ with isolated motoneurons and to explore cell type specific influence of $SOD1^{G93A}$.

EXPERIMENTAL PROCEDURES

Animals

B6.Cg-Tg(SOD1*G93A)1Gur/J (Jackson Laboratory, USA) and *Hb9::GFP* mice (T.M. Jessell's laboratory, Columbia University, NY, USA) were maintained on a C57BL/6J background under specific-pathogen-free conditions . All animal experiments were approved by the national ethics committee on animal experimentation, and were done in compliance with the European community and national directives for the care and use of laboratory animals. 11 mice were used for myoblasts banks and 9 pregnant mice for embryonic motoneuron primary cultures.

Motoneuron culture

Motoneuron cultures were isolated from the spinal cord of *Hb9::GFP* and *SOD1^{G93A}* mice at embryonic day (E) 12.5 (Raoul et al., 2002). Ventral part of the spinal cord from GFP-positive and GFP-negative littermate embryos were collected, pooled separately and dissociated mechanically following trypsin treatment. Cell homogenate obtained from *Hb9::GFP* spinal cords were then submitted to iodixanol density gradient centrifugation to enrich in motoneurons. In order to facilitate the development of spontaneous activity in culture while being able to easily visualize the motoneurons for electrophysiological recording, *Hb9::GFP* motoneurons are seeded with the total GFP-negative fraction (containing also glial cells and interneurons).

Myoblast isolation and differentiation

For primary culture of satellite cells, we used the offspring of female C57BL/6J and male *SOD1^{G93A}* mice. Five wild type (WT) and six *SOD1^{G93A}* primary cultures were generated for this study. Satellite cells were obtained from hind limb muscles of 3-4 weeks old mice (pre-symptomatic for SOD1^{G93A}). After mincing muscles, an enzymatic digestion was performed in Ham's F10 medium (ThermoFisher Scientific) supplemented with 2.5 mM $CaCl_2$, 0.5 mg/ml dispase II (Sigma-Aldrich) and 10 mg/ml collagenase B (Sigma-Aldrich). Following 15 min incubation twice at 37°C, a mechanical dissociation was performed. Muscle digest was passed through a 70 µm mesh filter, transferred to a 15 ml tube and spinned 5 min at 1000 rpm. The pellet was diluted in culture medium (Ham's F10, 20% fetal bovine serum, 2% penicillin/streptomycin, 2.5 ng/ml recombinant human fibroblast growth factor-basic (bFGF, ThermoFisher Scientific) and placed in a 60 mm diameter uncoated plastic plate for 1 hr to favor fibroblasts adherence. Afterwards, the medium solution was then removed and transferred into a plate coated with collagen at 37°C, 7 % CO_2. Satellite cells were allowed to multiply until they reach 70-80 % confluence and then split with 0.25 % trypsin to enhance the colony. Experiments were performed from third to fifth passage. For myoblasts differentiation and fusion, the serum was decreased to 2%.

Co-cultures

For motoneuron-myotube co-cultures, myoblasts were seeded on glass coverslips (1.5 cm^2) coated with poly-ornithine-laminin at a density of 10,000 /cm^2. After 2-3 days in multiplication medium, the medium was removed and motoneurons were added (1,700 / cm^2) in Neurobasal (Fisher Scientific) medium containing neurotrophic factors (1 ng/ml BDNF, 100 pg/ml GDNF, and 10 ng/ml CNTF), completed with 2% horse serum, 2% B27 supplement (ThermoFisher Scientific), 50 µM L-glutamine, 25 µM L-glutamate, and 25 µM β-mercaptoethanol. The low serum concentration of motoneuron culture medium allows the differentiation of myoblasts into myotubes. The co-culture was maintained at 37°C, in humidified incubator 93% O_2-7% CO_2 for 7-8 days before experiments to allow motoneurons electrical maturation.

Electrophysiology

Spontaneous electrical activity of motoneurons and myotubes was recorded with the loose-patch technique at room temperature using an Axopatch 200B amplifier (Molecular Devices). The bathing solution contained 145 mM NaCl, 5 mM KCl, 2 mM $CaCl_2$, 1.5 mM $MgCl_2$, 10 mM glucose and 10 mM HEPES, adjusted to pH 7.35. For excitatory post-synaptic potentials visualization, the motoneuron spontaneous electrical activity was recorded under whole-cell patch clamp with the patch pipette containing 8 mM KCl, 135 mM K-methane-sulfonate, 2 mM Mg-ATP, 0.5 mM Na-GTP, 0.1 mM EGTA and 10 mM HEPES, adjusted to pH 7.35. For loose-patch technique, the electrode was filled with the extracellular solution and the contact with cell membrane was in the range 30-80 MΩ. 6-cyano-7-nitroquinoxaline-2,3-dione (CNQX), d-tubocurarine (d-TC), tetrodotoxin (TTX) were purchased from Sigma-Aldrich.

Videomicroscopy

For live imaging, myotube contractions were recorded with the high-speed Orca-flash 4.0LT CCD camera (Hamamatsu Photonics) coupled with HCImage DIA software and connected to the inverted microscope used for electrophysiology. Acquisition period was 30 sec (28 fps). Phase contrast images of live cultures were acquired with the CCD camera.

Immunocytochemistry

Primary cultures at 7-8 DIV were fixed for 15 min in 4% paraformaldehyde in PBS, and incubated for 20 min in 15% donkey serum in PBS. They were then incubated 2 h at room temperature with the primary antibodies. After a wash in PBS, cultures were incubated for 1h at room temperature with secondary antibodies. After three washes in PBS, 10 min each, they were mounted in Mowiol. alpha-bungarotoxin Alexa Fluor 555 conjugate (1:1000, ThermoFisher Scientific) was added at the last wash before mounting. Primary antibodies were chicken anti-GFP to enhance staining of *Hb9*::*GFP* neurons (1:3000, Abcam); mouse anti-myosin heavy chain, MHC (clone A4.1025, 1:100, Developmental Studies Hybridoma Bank), mouse anti-rapsyn (1:100, Abcam), mouse anti-S100β (1:100, Novus Biologicals), goat anti-vesicular acetylcholine transporter (VAChT) (1:400, Merck Millipore), guinea pig anti-vesicular glutamate transporter 2 (VGluT2) (1:1000, synaptic systems). Fluorochrome-conjugated secondary antibodies (ThermoFisher Scientific) were used at 1:1000. Images were collected using Zeiss 40X EC Plan Neofluar 1.3NA oil objective.

RNA extraction and RT-qPCR

Myoblasts were seeded at the density of 10,000 /cm^2 in 60 mm diameter dishes. Total mRNA was extracted 2-3 days after seeding in multiplication medium and at 7 DIV after changing to a differentiation medium with the RNeasy Mini Kit (Qiagen). Following 2 min incubation in lysis buffer, 70% ethanol was added to equal volume and total mRNA was obtained using RNeasy minispin columns. The eluted mRNA was quantified by spectrophotometry (Nanodrop 2000, ThermoFisher Scientific). Following

genomic DNA wipe out, reverse transcription (RT) was performed with 1 µg of mRNA with the Quantitect RT kit (Qiagen). The collected cDNA was diluted to 100 ng with water and stored at -20°C until use. Primers were designed with Primers 3.0 software. Quantitative PCR was performed on 5 or 10 ng cDNA with SYBR Green (Qiagen) for detection and the LightCycler system (Roche Diagnostics). After initial activation for 15 min at 95°C, 45 cycles of 94°C for 15 s, 60°C for 20 s and 72°C for 35 s were carried out. After PCR amplification, a melting curve analysis was carried out to check PCR specificity. Polymerase (RNA) II polypeptide J (*Polr2J*) levels were used to normalize the amounts of cDNA. ΔC_t was calculated as the differences between the Ct values, determined with the equation 2–ΔCt. Primers sequences are given in Table 1.

Statistics

Data are presented as means ± standard error of the mean (SEM) or as median for non-parametric test. Statistical significance was accepted at the level of $p < 0.05$. Unpaired or paired two-tailed *t* test, X^2 square and Mann-Whitney test were used when appropriate.

RESULTS

Pharmacological profile of spontaneous activity of motoneurons and myotubes in primary culture

Before assessing the formation of a functional NMJ in motoneuron-myotubes co-cultures, we aimed to set the phenotypic and pharmacological characteristics of each culture. We previously shown that, from 7 days *in vitro* (DIV), cultured primary motoneurons display adult-like intrinsic electrical activity (Bowerman et al., 2017). In primary culture, We isolated motoneurons from mice expressing GFP under the control of the motoneuron-selective *Hb9* promoter (*Hb9::GFP*) to facilitate motoneuron identification. *Hb9::GFP* motoneurons express the vesicular acetylcholine transporter (VAChT) a cholinergic marker and the vesicular glutamate transporter 2 (VGluT2), a glutamatergic marker (Fig. 1A, left panel). This observation is in agreement with studies showing that motoneurons have not a single neurotransmitter phenotype and can release both Acetylcholine and Glutamate (Nishimaru et al., 2005, Lamotte d'Incamps et al., 2017). The *Hb9::GFP* negative neurons express only VGluT2, identifying putative glutamatergic interneurons (Fig.1A, right panel). The primary culture also contains glial cells expressing the S100β marker, which can be observed in close vicinity of the motoneurons (Fig. 1B). Using loose patch-clamp technique, a spontaneous electrical activity was recorded in GFP-positive motoneurons (Fig. 1B, C). The probability to record a spontaneous activity at 7-8 DIV was strongly increased using a mixed ventral horn culture composed of motoneurons, interneurons and glial cells. Thereafter, we used mixed ventral horn cultures for all experiments. The basal spontaneous frequency was 0.53 ± 0.12 Hz, $n = 22$. This spontaneous activity was inhibited following addition of 50 µM 6-cyano-7-nitroquinoxaline-2,3-dione (CNQX) to block AMPA/kainate receptors, but was not modified by 50 µM d-tubocurarine (d-TC) that blocks nicotinic receptors. These observations support that motoneuron spontaneous activity is under a glutamatergic network-driven activity as reported in (Ullian et al., 2004) (Fig. 1D, E).

After 7-8 DIV in differentiation medium and despite the absence of motoneurons, a small proportion of myotubes displays spontaneous contractions as assessed during 30 min observation per well (3.7 ± 1.3 contracting myotubes per well, *n* = 3 cultures). These spontaneous contractions have already been attributed to maturation of electrical activity of mouse myotubes (Lorenzon et al., 2002, Das et al., 2009). Using videomicroscopy for contraction recordings (Fig. 1F and Movie 1), we show that the contraction frequency was of 1.7 ± 0.2 Hz, *n* =10. Myotubes spontaneous contractions were not inhibited by CNQX (Fig. 1 G, H), while application of d-TC induced a fibrillation-like pattern characterized by an increase in contraction frequency associated with a decrease in amplitude, leading in most cases to a contracture (Fig. 1 G, H and Movie 1). This observation is in agreement with previous studies that reported that d-TC can have fibrillary effect on denervated muscle and depolarizes embryonic muscle fibers (Ziskind and Dennis, 1978, Smith et al., 2013). In all cases, application of 1 µM TTX totally inhibited spontaneous contractions. (Fig. 1 G, H and Movie 1). Coupling videomicroscopy recordings of myotubes contractions with extracellular recordings of their electrical activity confirmed that each contraction is associated with an electrical spike (Fig. 1 I).

From these data, we selected CNQX, as a specific inhibitor of synaptic-driven neuronal activity, to assess the formation of neuron-driven contractions.

Co-cultured myotubes-motoneurons increase neuronal network activity, but not contraction frequency of myotubes

We next analyzed the effects of the presence of motoneurons on the spontaneous activity of myotubes. Addition of wild-type (WT) motoneurons to myotube culture induces a two-fold increase in the number of myotubes having contractions (Fig. 2A). To assess the formation of NMJ, a morphological analysis was performed using fluorochrome-conjugated alpha-bungarotoxine (αBTX) to label nicotinic acetylcholine receptors. The staining was evident as clusters on most myotubes, while apposition with process endings of motoneurons, labelled with GFP, was observed only in few myotubes (Fig. 2B). NMJ expressed the post-synaptic marker of maturation Rapsyn in close proximity with αBTX and the neuronal pre-synaptic VAChT shows close apposition with the nicotinic receptors (Fig. 2 C) with a morphology consistently observed *in vitro* (Zahavi et al., 2015, Vilmont et al., 2016). Spontaneous electrical activity of myotube (contracting myotube) and motoneurons was recorded using loose-patch clamp (Fig. 2 C, D). The electrical activity frequency of WT contracting myotubes in co-culture was 1.7 ± 0.2 Hz, *n* = 27, a value similar to the spontaneous contraction frequency (Fig. 2 E), while in the presence of WT myotubes, there was a significant three-fold increase in motoneuron spontaneous firing frequency (Fig. 2F).

***SOD1^{G93A}* myotubes display reduced contraction frequency**

To assess the effect of SOD1^{G93A} mutant on myotube contraction frequency, myotubes obtained from muscle satellite cells of *SOD1^{G93A}* mice were analyzed in the presence of WT motoneurons. Mutant myotubes display a significantly two-fold lower contraction-associated spike frequency than WT (Fig. 3A). To verify whether the mutation could disrupt the functional link between contraction and electrical

frequency, we combined videomicroscopy with loose patch recordings and found that, similarly to what observed with WT myotubes, each contraction of *SOD1^{G93A}* myotube was associated with an electrical spike (Fig. 3B, C). Analysis of the time for the contraction-relaxation cycle revealed no significant differences between WT and mutant myotubes (550 ± 57 ms, n = 13 and 621 ± 66 ms, n = 14 for WT and mutant myotubes, respectively (two-tailed t test $t_{(25)} = 0.807$, $p \geq 0.05$; $F_{(13,12)} = 1.458$ $p \geq 0.05$). Furthermore, the presence of *SOD1^{G93A}* myotubes, does not modify the spontaneous firing frequency of WT motoneurons as compared with WT myotubes (1.3 ± 0.3 Hz, n = 20, from 3 co-cultures) (Fig. 3D). Thus, *SOD1^{G93A}* myotubes display lower contraction frequency than WT that appears to not be associated with changes in motoneuron electrical network or in contraction-relaxation duration.

SOD1^{G93A} reduces the expression of the slow myosin heavy chain isoform in myotubes

Contraction is dependent on myotube maturation state and expression of myosin heavy chain (MHC) isoforms (Schiaffino and Reggiani, 2011). Therefore, we investigated the process of WT and *SOD1^{G93A}* myoblasts differentiation *in vitro* using the expression of the transcription factor, *paired box 7* (*Pax7*), a marker of myoblasts proliferation (Dumont et al., 2015) and *creatine kinase* muscle isoform (*Ckm*) a myogenic differentiation marker. Quantitative PCR on myoblasts culture (Fig. 4A) and 7 days after the induction of differentiation (Fig. 4B) shows similar changes in *Pax7* and *Ckm* levels of expression between WT and *SOD1^{G93A}* (Fig. 4C, D). These results suggest that the maturation process *in vitro* is not modified by the mutation.

We next analyzed the expression of different MHC isoform transcripts during differentiation, as they are major markers of skeletal fibers types (Schiaffino and Reggiani, 2011). During the process of differentiation, the expression of the skeletal muscle embryonic myosin heavy chain isoform, *Mhy3,* remained unchanged and there was a significant increase in the *Myh8* neonatal isoform (Fig. 4E, F). Analysis of the three adult isoforms*, Myh2*, *4* and *7*, displayed no significant changes in the fast fatigue resistant type II-a isoform, *Myh2*, expression during differentiation (Fig. 4G), while there was a significant increase in the transcript expression of the fast fatigable type II-b isoform, *Myh4,* during differentiation of both WT and *SOD1^{G93A}* myotubes (Fig. 4H). In addition, the slow type I isoform, *Myh7*, expression levels were significantly decreased during differentiation of SOD1^{G93A}-expressing myotubes (Fig. 4I). Additional analysis of *Myh7* expression in WT and *SOD1^{G93A}* myoblasts shows no significant differences in median values, supporting further a decrease during the differentiation process of *SOD1^{G93A}* myoblasts (Mann-Whitney test, $U_{(6,6)} = 16.5$, $p \geq 0.05$). Altogether, these results demonstrate that myoblast differentiation *in vitro* mainly drives the expression of the neonatal and fast fatigable II-b fiber markers both in WT and SOD1 mutant myotubes. Interestingly, SOD1^{G93A} expression in myotubes decreases the level of the slow type fiber marker *Myh7*.

SOD1^{G93A} expression in motoneurons impairs formation of functional NMJ

To evidence whether functional NMJs were formed, we analyzed the effects of CNQX on the contracting myotubes as this pharmacological agent selectively inhibits the ionotropic glutamatergic drive of motoneuron activity and does not modify spontaneous contractions. CNQX inhibited contractions in 89

% of WT myotubes (8 out of 9, from 2 different co-cultures). The effects of d-TC on co-cultured myotubes were similar to those observed in aneurally cultured myotubes, *i.e*. it induces a strong decrease in amplitude of contraction associated with a fibrillation-like pattern in the frequency from 1.4 ± 0.1 Hz to 4.0 ± 1.0 Hz (*n* = 3 myotubes, 1 culture, not shown). These results suggest that myotube contraction in co-culture is due to acetylcholine release driven by glutamate depolarization of motoneurons (Fig. 5A, E). In *SOD1^{G93A}* myotubes, CNQX inhibited contractions in 78 % of myotubes (13 out of 18, from 3 different co-cultures), this inhibition being not significantly different from that observed with WT myotubes (Fig. 5B, E). To reproduce the *in vivo* configuration and in order to answer the question of whether SOD1 mutation in spinal cord could influence neurotransmission at the NMJ, SOD1^{G93A}-expressing myotubes were co-cultured with neuronal culture from the ventral horn of *SOD1^{G93A}* spinal cord. Under this condition, CNQX inhibited contractions in only 22 % of mutated myotubes (2 out of 11, from 2 different co-cultures)(Fig. 5C, E). Lastly, to assess whether neuronal expression of SOD1^{G93A} is a condition sufficient for reducing the functional formation of a NMJ, mutated neuronal culture was co-cultured with WT myotubes. Under this condition, CNQX inhibited 11 % of WT myotube contractions (1 out of 9, from 3 different co-cultures) (Fig. 5D, E). Altogether, these results support that spinal SOD1^{G93A} expression is a major contributor to the loss of neurotransmission at the NMJ.

DISCUSSION

Here, we describe a co-culture model that recapitulates both developmental and injury-associated regenerative synaptogenesis and allows discriminating the effects of ALS-causing protein on muscular function. We show that enrichment with interneurons and glial cells increases the frequency of excitatory synaptic activity, which could be attributed in part to glial cells known to increase the number of glutamatergic ionotropic receptors (Ullian et al., 2004). In addition to the well-known trophic effects of muscle-derived factors on motoneuron survival, (Oppenheim, 1989, Arce et al., 1998), our results indicate that even in the presence of neurotrophic factors, glia and interneurons, the addition of myotubes increases the spontaneous firing frequency of motoneurons suggesting that myotubes do also add to the maturation of the glutamate-driven network. Expression of *SOD1^{G93A}* in myotubes does not modify the spontaneous firing of motoneurons, suggesting that the ALS-linked mutant protein does not alter the influence of myotube on motoneuron network maturation. However, mutant myotubes present lower contraction frequency than WT supporting intrinsic modifications induced by *SOD1^{G93A}* expression (Dobrowolny et al., 2008).

To decipher molecular basis for the decreased contraction frequency in mutant myotubes, we analyzed the intrinsic potential of MHC isoforms to differentiation towards adult isoforms. Our data show that, *in vitro*, myotubes from both genotypes mainly increase fast fatigable type II-b *Myh4* expression of MHC during maturation, which suggests that our culture system fosters the glycolytic pathway over the oxidative. In a previous study, we showed that, independently of intrinsic maturation, the level of the two adult fast isoforms *Myh2* and *Myh4* expression is lower in mutant myotubes (Varga et al., 2018). So, independently of gene expression levels, the major up-regulation of the fast fatigable type II-b *Myh4* isoform could be a factor influencing contraction frequency in mutant myotubes. Indeed, early muscle

intrinsic metabolic alterations of the fast isoforms are reported in ALS mice including altered glucose metabolism and a metabolic switch towards lipid use (Smittkamp et al., 2014, Palamiuc et al., 2015, Dobrowolny et al., 2018). The fast fiber type shows high shortening velocity and overexpressed SOD1^{G93A} influences their contractile properties towards slower relaxation (Derave et al., 2003), which could contribute to the lower contraction frequency of SOD1^{G93A} myotubes. However, the lack of differences in contraction duration between WT and mutant myotubes does not support this hypothesis. In addition to the fast isoforms, we show that the slow *Myh7* isoform expression is decreased in mutant myotubes during the process of maturation and has a trend towards a decrease in mutant myotubes compared with WT (Varga et al., 2018). Therefore, this isoform appears to be the most affected by the mutation with an overall decrease in its expression level. From a functional point of view, this isoform is regulated by calcineurin, a molecular decoder of sustained intracellular Ca^{2+} signals that occurs during contractions (Olson and Williams, 2000). Therefore, *Myh7* could be a marker of myotubes and myoblasts having spontaneous contractions. Its reduced expression in SOD1^{G93A} myotubes agrees with the decrease in calcineurin activity in ALS (Ferri et al., 2004) and suggests that SOD1^{G93A} myotubes are less excitable. Muscle excitability threshold is dependent on numerous factors including the fiber type, the slow type having the lowest threshold (Pierno et al., 2002), the muscle ionic channels whose expression is modified in ALS mice (Camerino et al., 2019). Synaptic strength of motor units of fast and slow muscle fibers is also differentially affected by SOD1 mutation early in the disease (Tremblay et al., 2017), which could account for a reduced contraction frequency in mutant myotubes provided that the fast type Myh4 expression dominates myotube contractions. Biophysical factors such the rheological properties that comprise cell elasticity could also influence the contractile dynamics. In support to this, using atomic force microscopy, we reported that mutant myotubes display a hardest structure than WT which could contribute to reduced contraction dynamics (Varga et al., 2018).

In agreement with the formation of functional NMJs, we show that addition of motoneurons increases the number of contracting myotubes and 89% of them were sensitive to CNQX inhibition. When SOD1^{G93A} is overexpressed in myotubes, there was a trend towards a decrease in the occurrence of CNQX-sensitive contraction to 78% of myotubes which was however not significant and supports that the process of neurotransmission is not merely affected by muscle SOD1^{G93A} expression. In contrast, expression of SOD1 mutant in motoneurons greatly decreases the probability to make a functional synapse with SOD1^{G93A}-expressing myotubes to 22% of CNQX-sensitive contractions. The formation and stability of a NMJ depend on factors secreted by motoneurons (Sanes and Lichtman, 2001). Recently, expression of Wnt3 protein by motoneurons was shown to promote the aggregation of acetylcholine receptors on muscles (Henriquez et al., 2008, Shen et al., 2018). Interestingly, decreased expression of Wnt3 has been reported in ALS limb muscles (McLoon et al., 2014). The overall process of motoneuronal secretion, including neurotransmitter release, alongside a slowing of vesicular transport could also contribute to the delay in myotube innervation (Williamson and Cleveland, 1999). Moreover, impaired re-innervation following nerve crush is shown in SOD1^{G93A} mice which could also explain the delay or loss of innervation we observe in our mixed developmental and injury-associated regenerative synaptogenesis (Pun et al., 2006, Schram et al., 2019). Indeed, these studies show that mutant motoneurons have a reduced capacity to regeneration following peripheral injury. In addition to intrinsic

deficiency, mutant astrocytes display toxic effects on motoneurons which probably contributes to the reduced functional NMJ induced by neuronal SOD1^{G93A} culture (Aebischer et al., 2011, Yamanaka and Komine, 2018).

In conclusion, this study provides relevant information on the development of neuromuscular defects during ALS progression. Our results strongly support that diseased motoneurons are a major factor involved in the process of NMJ dismantlement in the SOD1^{G93A} ALS model.

ACKNOWLEDGEMENTS

We are grateful to the Montpellier RIO Imaging and the INM animal facility for their services. This work was supported by grants from the Institut National de la Santé et de la Recherche Médicale (Inserm), the association pour la recherche sur la SLA (ARSLA, grant number R14071FF), ANR Mimetic (grant number 15-CE18-0017), association française contre les myopathies (AFM, grant number 19496) and LabEx NUMEV (ANR-10-LABX-20). R.Y. is supported by Lebanese University (PhD fellowships). M.B. was an EMBO Long-Term Fellow whilst at the INM.

CONFLICT OF INTEREST STATEMENT

The authors declare that they have no conflict of interest.

AUTHOR CONTRIBUTION

F.S and C.H designed the research

S.B, A.S-V, V.M, R.Y, O.L, C.S, R.Y, M.B, C.H, F.S performed the research

C.G, M.B, C.R, C.H, F.S analyzed the data

F.S, C.H and C.R wrote the manuscript

REFERENCES

Aebischer, J., Cassina, P., Otsmane, B., Moumen, A., Seilhean, D., Meininger, V., Barbeito, L., Pettmann, B. and Raoul, C., 2011. IFNgamma triggers a LIGHT-dependent selective death of motoneurons contributing to the non-cell-autonomous effects of mutant SOD1. Cell Death Differ. 18, 754-768.

Arce, V., Pollock, R. A., Philippe, J. M., Pennica, D., Henderson, C. E. and Delapeyriere, O., 1998. Synergistic effects of Schwann- and muscle-derived factors on motoneuron survival involve GDNF and cardiotrophin-1 (CT-1). J Neurosc. 18, 1440-1448.

Bowerman, M., Salsac, C., Bernard, V., Soulard, C., Dionne, A., Coque, E., Benlefki, S., Hince, P., Dion, P. A., Butler-Browne, G., Camu, W., Bouchard, J. P., Delpire, E., Rouleau, G. A., Raoul, C. and Scamps, F., 2017. KCC3 loss-of-function contributes to Andermann syndrome by inducing activity-dependent neuromuscular junction defects. Neurobiol Dis. 106, 35-48.

Camerino, G. M., Fonzino, A., Conte, E., De Bellis, M., Mele, A., Liantonio, A., Tricarico, D., Tarantino, N., Dobrowolny, G., Musaro, A., Desaphy, J. F., De Luca, A. and Pierno, S., 2019. Elucidating the Contribution of Skeletal Muscle Ion Channels to Amyotrophic Lateral Sclerosis in search of new therapeutic options. Sci Rep. 9, 3185.

Charge, S. B. and Rudnicki, M. A., 2004. Cellular and molecular regulation of muscle regeneration. Physiol Rev. 84, 209-238.

Da Cruz, S., Parone, P. A., Lopes, V. S., Lillo, C., McAlonis-Downes, M., Lee, S. K., Vetto, A. P., Petrosyan, S., Marsala, M., Murphy, A. N., Williams, D. S., Spiegelman, B. M. and Cleveland, D. W., 2012. Elevated PGC-1alpha activity sustains mitochondrial biogenesis and muscle function without extending survival in a mouse model of inherited ALS. Cell Metab. 15, 778-786.

Das, M., Rumsey, J. W., Bhargava, N., Stancescu, M. and Hickman, J. J., 2009. Skeletal muscle tissue engineering: a maturation model promoting long-term survival of myotubes, structural development of the excitation-contraction coupling apparatus and neonatal myosin heavy chain expression. Biomaterials. 30, 5392-5402.

Derave, W., Eijnde, B. O. and Hespel, P., 2003. Creatine supplementation in health and disease: what is the evidence for long-term efficacy? Mol Cell Biochem. 244, 49-55.

Dobrowolny, G., Aucello, M., Rizzuto, E., Beccafico, S., Mammucari, C., Boncompagni, S., Belia, S., Wannenes, F., Nicoletti, C., Del Prete, Z., Rosenthal, N., Molinaro, M., Protasi, F., Fano, G., Sandri, M. and Musaro, A., 2008. Skeletal muscle is a primary target of SOD1G93A-mediated toxicity. Cell Metab. 8, 425-436.

Dobrowolny, G., Lepore, E., Martini, M., Barberi, L., Nunn, A., Scicchitano, B. M. and Musaro, A., 2018. Metabolic Changes Associated With Muscle Expression of SOD1(G93A). Front Physiol. 9, 831.

Dumont, N. A., Wang, Y. X. and Rudnicki, M. A., 2015. Intrinsic and extrinsic mechanisms regulating satellite cell function. Development. 142, 1572-1581.

Dupuis, L., Gonzalez de Aguilar, J. L., Echaniz-Laguna, A., Eschbach, J., Rene, F., Oudart, H., Halter, B., Huze, C., Schaeffer, L., Bouillaud, F. and Loeffler, J. P., 2009. Muscle mitochondrial uncoupling dismantles neuromuscular junction and triggers distal degeneration of motor neurons. PLoS One. 4, e5390.

Ferri, A., Nencini, M., Battistini, S., Giannini, F., Siciliano, G., Casali, C., Damiano, M. G., Ceroni, M., Chio, A., Rotilio, G. and Carri, M. T., 2004. Activity of protein phosphatase calcineurin is decreased in sporadic and familial amyotrophic lateral sclerosispatients. J Neurochem. 90, 1237-1242.

Henriquez, J. P., Webb, A., Bence, M., Bildsoe, H., Sahores, M., Hughes, S. M. and Salinas, P. C., 2008. Wnt signaling promotes AChR aggregation at the neuromuscular synapse in collaboration with agrin. Proc Natl Acad Sci U S A. 105, 18812-18817.

Lamotte d'Incamps, B., Bhumbra, G. S., Foster, J. D., Beato, M. and Ascher, P., 2017. Segregation of glutamatergic and cholinergic transmission at the mixed motoneuron Renshaw cell synapse. Sci Rep. 7, 4037.

Loeffler, J. P., Picchiarelli, G., Dupuis, L. and Gonzalez De Aguilar, J. L., 2016. The Role of Skeletal Muscle in Amyotrophic Lateral Sclerosis. Brain Pathol. 26, 227-236.

Lorenzon, P., Bernareggi, A., Degasperi, V., Nurowska, E., Wernig, A. and Ruzzier, F., 2002. Properties of primary mouse myoblasts expanded in culture. Exp Cell Res. 278, 84-91.

Maimon, R., Ionescu, A., Bonnie, A., Sweetat, S., Wald-Altman, S., Inbar, S., Gradus, T., Trotti, D., Weil, M., Behar, O. and Perlson, E., 2018. miR126-5p Downregulation Facilitates Axon Degeneration and NMJ Disruption via a Non-Cell-Autonomous Mechanism in ALS. J Neurosc. 38, 5478-5494.

Manzano, R., Toivonen, J. M., Calvo, A. C., Olivan, S., Zaragoza, P., Rodellar, C., Montarras, D. and Osta, R., 2013. Altered in vitro proliferation of mouse SOD1-G93A skeletal muscle satellite cells. Neurodegener Dis. 11, 153-164.
McLoon, L. K., Harandi, V. M., Brannstrom, T., Andersen, P. M. and Liu, J. X., 2014. Wnt and extraocular muscle sparing in amyotrophic lateral sclerosis. Invest Ophthalmol Vis Sci. 55, 5482-5496.
Nishimaru, H., Restrepo, C. E., Ryge, J., Yanagawa, Y. and Kiehn, O., 2005. Mammalian motor neurons corelease glutamate and acetylcholine at central synapses. Proc Natl Acad Sci U S A. 102, 5245-5249.
Olson, E. N. and Williams, R. S., 2000. Calcineurin signaling and muscle remodeling. Cell. 101, 689-692.
Oppenheim, R. W., 1989. The neurotrophic theory and naturally occurring motoneuron death. Trends Neurosci. 12, 252-255.
Palamiuc, L., Schlagowski, A., Ngo, S. T., Vernay, A., Dirrig-Grosch, S., Henriques, A., Boutillier, A. L., Zoll, J., Echaniz-Laguna, A., Loeffler, J. P. and Rene, F., 2015. A metabolic switch toward lipid use in glycolytic muscle is an early pathologic event in a mouse model of amyotrophic lateral sclerosis. EMBO Mol Med. 7, 526-546.
Pierno, S., Desaphy, J. F., Liantonio, A., De Bellis, M., Bianco, G., De Luca, A., Frigeri, A., Nicchia, G. P., Svelto, M., Leoty, C., George, A. L., Jr. and Camerino, D. C., 2002. Change of chloride ion channel conductance is an early event of slow-to-fast fibre type transition during unloading-induced muscle disuse. Brain. 125, 1510-1521.
Pradat, P. F., Barani, A., Wanschitz, J., Dubourg, O., Lombes, A., Bigot, A., Mouly, V., Bruneteau, G., Salachas, F., Lenglet, T., Meininger, V. and Butler-Browne, G., 2011. Abnormalities of satellite cells function in amyotrophic lateral sclerosis. Amyotroph Lateral Scler. 12, 264-271.
Pun, S., Santos, A. F., Saxena, S., Xu, L. and Caroni, P., 2006. Selective vulnerability and pruning of phasic motoneuron axons in motoneuron disease alleviated by CNTF. Nat Neurosci. 9, 408-419.
Raoul, C., Estevez, A. G., Nishimune, H., Cleveland, D. W., deLapeyriere, O., Henderson, C. E., Haase, G. and Pettmann, B., 2002. Motoneuron death triggered by a specific pathway downstream of Fas. potentiation by ALS-linked SOD1 mutations. Neuron. 35, 1067-1083.
Sanes, J. R. and Lichtman, J. W., 2001. Induction, assembly, maturation and maintenance of a postsynaptic apparatus. Nat Rev Neurosci. 2, 791-805.
Schiaffino, S. and Reggiani, C., 2011. Fiber types in mammalian skeletal muscles. Physiol Rev. 91, 1447-1531.
Schram, S., Chuang, D., Schmidt, G., Piponov, H., Helder, C., Kerns, J., Gonzalez, M., Song, F. and Loeb, J. A., 2019. Mutant SOD1 prevents normal functional recovery through enhanced glial activation and loss of motor neuron innervation after peripheral nerve injury. Neurobiol Dis. 124, 469-478.
Shen, C., Li, L., Zhao, K., Bai, L., Wang, A., Shu, X., Xiao, Y., Zhang, J., Zhang, K., Hui, T., Chen, W., Zhang, B., Hsu, W., Xiong, W. C. and Mei, L., 2018. Motoneuron Wnts regulate neuromuscular junction development. Elife. 7.
Smith, A. S., Long, C. J., Pirozzi, K. and Hickman, J. J., 2013. A functional system for high-content screening of neuromuscular junctions in vitro. Technology (Singap World Sci). 1, 37-48.
Smittkamp, S. E., Morris, J. K., Bomhoff, G. L., Chertoff, M. E., Geiger, P. C. and Stanford, J. A., 2014. SOD1-G93A mice exhibit muscle-fiber-type-specific decreases in glucose uptake in the absence of whole-body changes in metabolism. Neurodegener Dis. 13, 29-37.
Taylor, J. P., Brown, R. H., Jr. and Cleveland, D. W., 2016. Decoding ALS: from genes to mechanism. Nature. 539, 197-206.
Towne, C., Raoul, C., Schneider, B. L. and Aebischer, P., 2008. Systemic AAV6 delivery mediating RNA interference against SOD1: neuromuscular transduction does not alter disease progression in fALS mice. Mol Ther. 16, 1018-1025.
Tremblay, E., Martineau, E. and Robitaille, R., 2017. Opposite Synaptic Alterations at the Neuromuscular Junction in an ALS Mouse Model: When Motor Units Matter. J Neurosc. 37, 8901-8918.
Ullian, E. M., Harris, B. T., Wu, A., Chan, J. R. and Barres, B. A., 2004. Schwann cells and astrocytes induce synapse formation by spinal motor neurons in culture. Mol Cell Neurosci. 25, 241-251.
Varga, B., Martin-Fernandez, M., Hilaire, C., Sanchez-Vicente, A., Areias, J., Salsac, C., Cuisinier, F. J. G., Raoul, C., Scamps, F. and Gergely, C., 2018. Myotube elasticity of an amyotrophic lateral sclerosis mouse model. Sci Rep. 8, 5917.
Vilmont, V., Cadot, B., Ouanounou, G. and Gomes, E. R., 2016. A system for studying mechanisms of neuromuscular junction development and maintenance. Development. 143, 2464-2477.
Williamson, T. L. and Cleveland, D. W., 1999. Slowing of axonal transport is a very early event in the toxicity of ALS-linked SOD1 mutants to motor neurons. Nat Neurosci. 2, 50-56.
Wong, M. and Martin, L. J., 2010. Skeletal muscle-restricted expression of human SOD1 causes motor neuron degeneration in transgenic mice. Hum Mol Genet. 19, 2284-2302.

Yamanaka, K. and Komine, O., 2018. The multi-dimensional roles of astrocytes in ALS. Neurosci Res. 126, 31-38.
Zahavi, E. E., Ionescu, A., Gluska, S., Gradus, T., Ben-Yaakov, K. and Perlson, E., 2015. A compartmentalized microfluidic neuromuscular co-culture system reveals spatial aspects of GDNF functions. J Cell Sci. 128, 1241-1252.
Ziskind, L. and Dennis, M. J., 1978. Depolarising effect of curare on embryonic rat muscles. Nature. 276, 622-623.

SUPPLEMENTARY INFORMATION

Movie 1: Live imaging of myotube contractions showing the serial effects of CNQX, d-TC and TTX application. (15 fps).

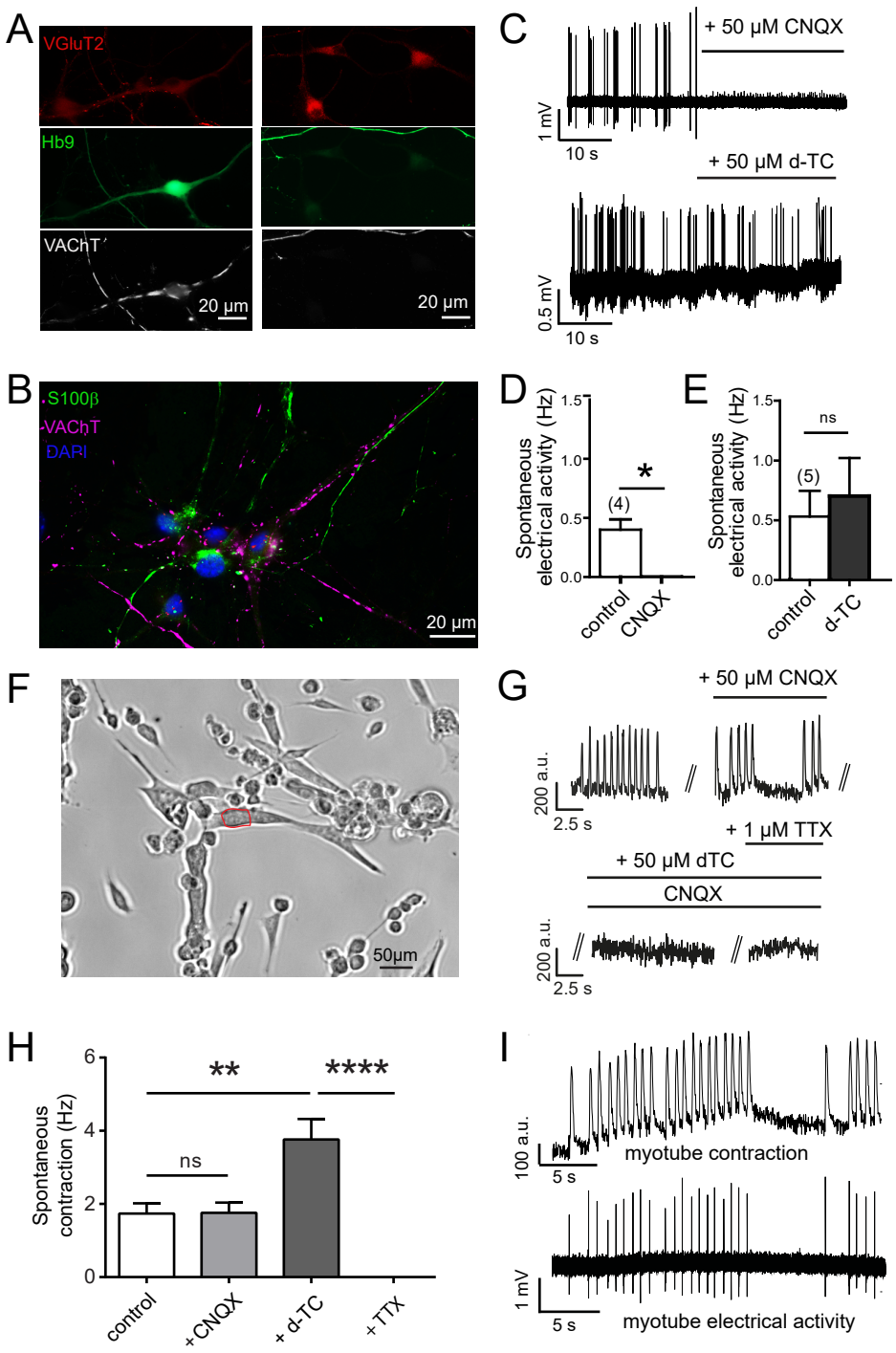

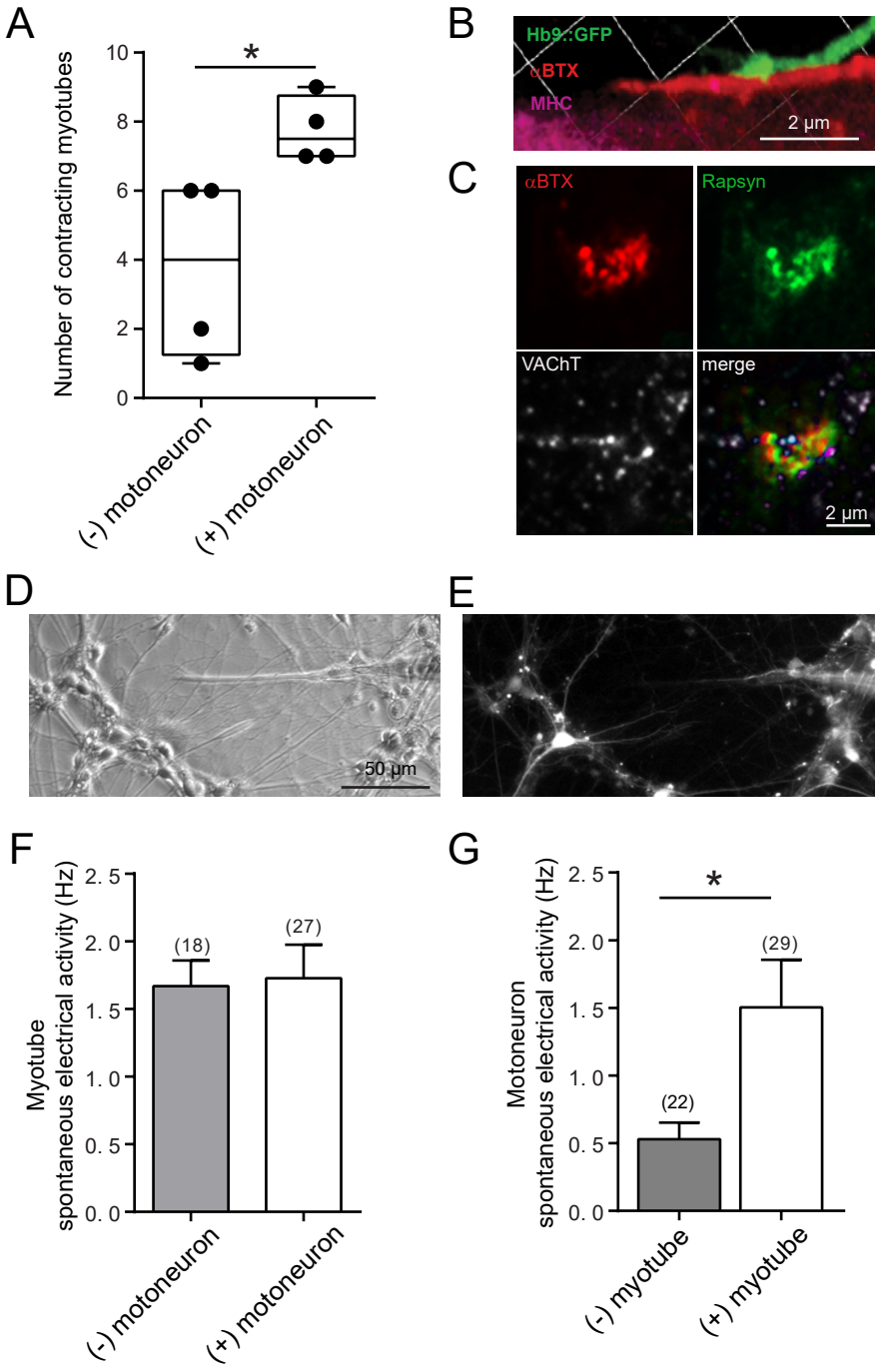

Figure 3

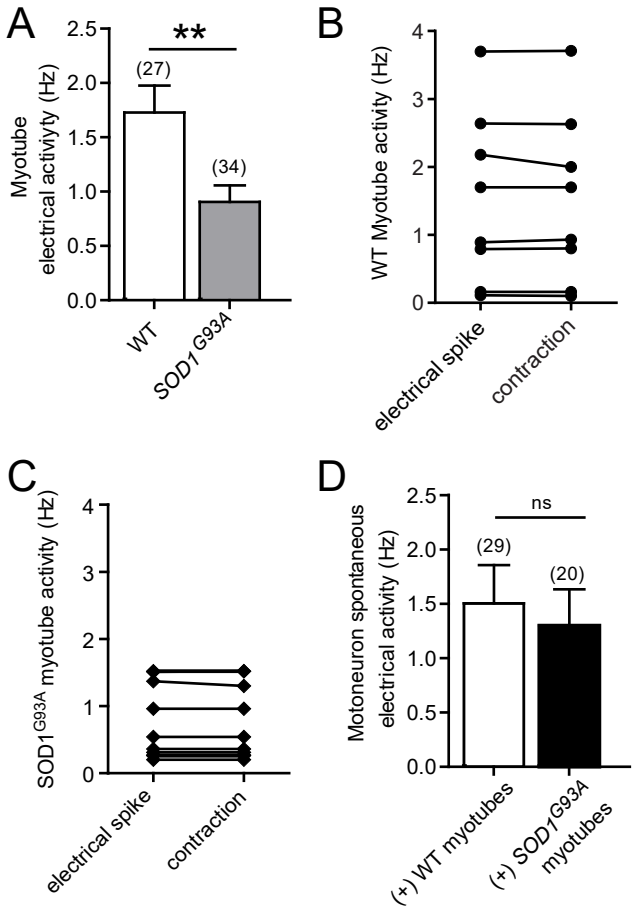

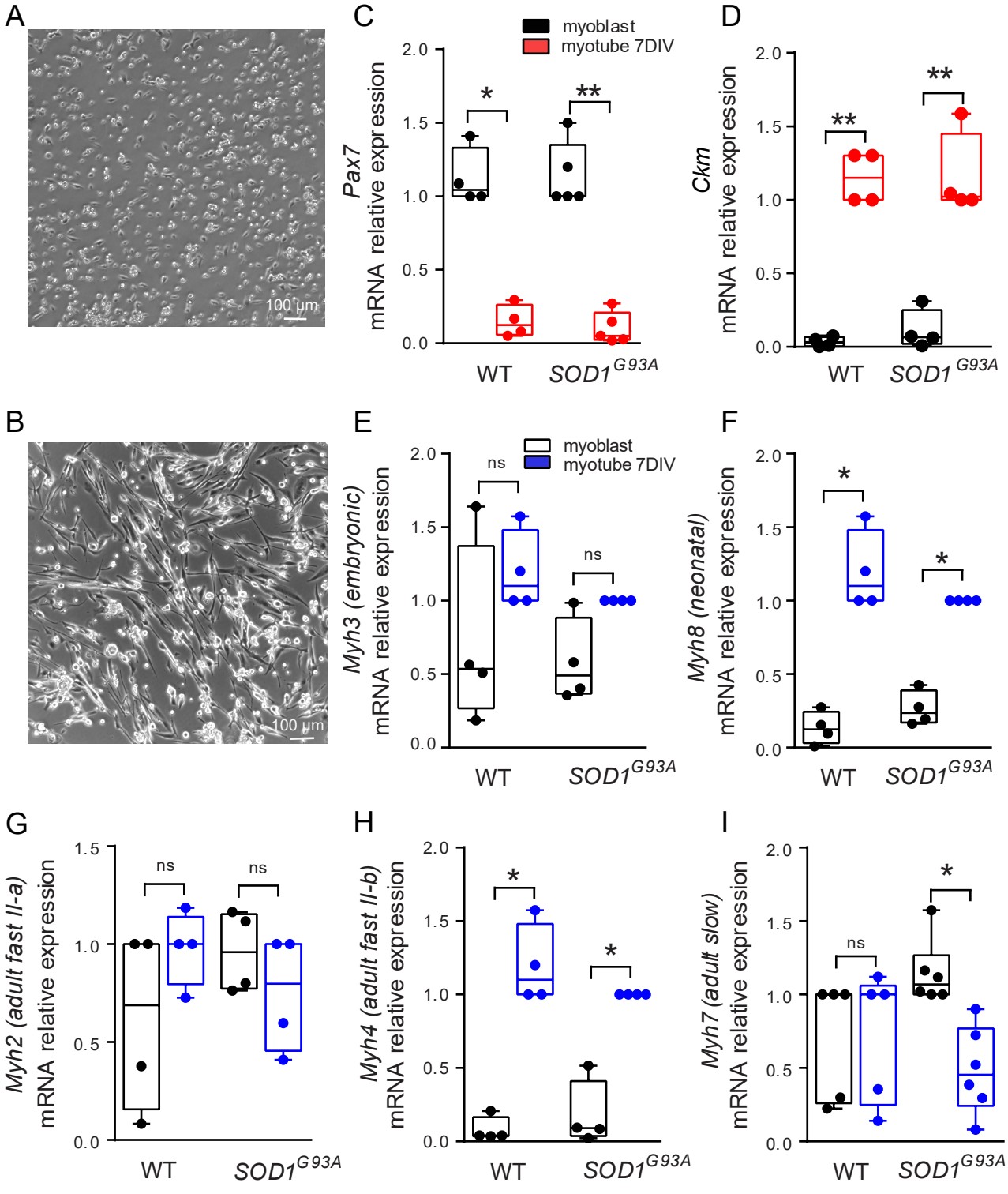

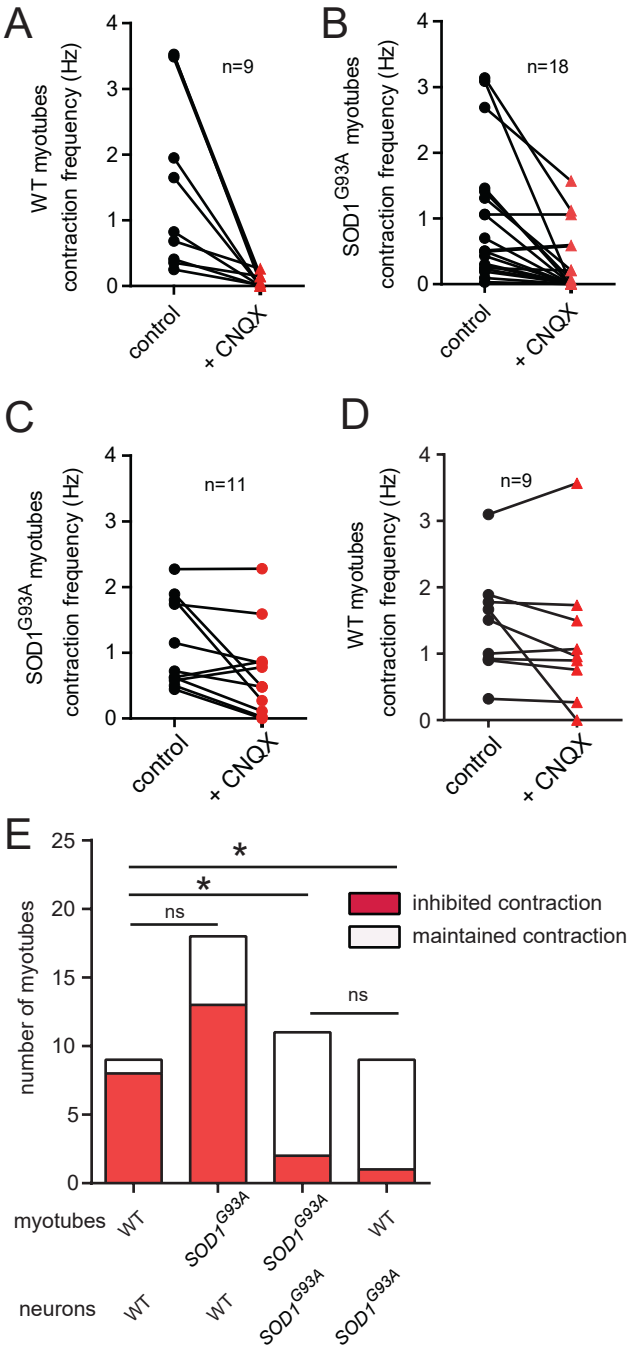

FIGURE LEGEND

Fig. 1. Pharmacological characterization of spontaneous activity of motoneurons and myotubes in primary culture. (A) Primary culture of ventral horn contains *Hb9::GFP* positive motoneurons showing co-expression with the cholinergic marker VAChT in soma and neurites. Motoneurons also express the glutamatergic marker, VGluT2 (left). *Hb9::GFP* negative interneurons express VGluT2, not VAChT (right). **(B)** Immunolabeling with the astrocyte marker S100β reveals the presence of glial cells in ventral horn culture. **(C)** Extracellular recordings of spontaneous electrical activity of 2 different motoneurons in the presence (or not) of the ionotropic glutamate receptor AMPA/Kainate inhibitor, CNQX or the ionotropic nicotinic receptor inhibitor, d-TC, with the loose patch technique. **(D)** Quantification of motoneuron spontaneous activity before (control) and following addition of 50 µM CNQX (paired, two-tailed *t* test, $t_{(3)} = 4.572$, $R^2 = 0.874$, $p \leq 0.05$). **(E)** Inhibition of nicotinic receptors with 50 µM d-TC has no effect on motoneuron spontaneous activity (paired, two-tailed *t* test, $t_{(4)} = 1.485$, $p \geq 0.05$). Values are means ± SEM, number of cells is in bracket. **(F)** Representative phase contrast image of 8 DIV primary myotube culture. Part of a contracting myotube is selected for live imaging (selection box in red). Changes in contrast in selected pixels due to myotube movement allows quantification of a contraction. **(G)** Illustration of contractions recordings of a myotube (control) and following CNQX, d-TC and TTX application (parallel bars indicates interruption of recordings during drug application). Note that the apparent noise increase of baseline under d-TC is actually due to myotube fibrillation (see corresponding movie 1). TTX further reduces baseline noise and stops contractions. **(H)** Analysis of myotube contraction frequency. Application of 50 µM CNQX does not modify spontaneous frequency (two-tailed *t* test, $t_{(18)} = 0.05$, $F_{(9,9)} = 1.003$, $p \geq 0.05$). Inhibition of nicotinic receptors with 50 µM d-TC induces low amplitude, high frequency contractions (two-tailed *t* test, $t_{(17)} = 3.344$, $R^2 = 0.396$, $p \leq 0.01$; $F_{(8,9)} = 3.571$, $p \geq 0.05$). Addition of 1 µM TTX that inhibits electrical activity stops the low amplitude, high frequency contractions (two-tailed *t* test, $t_{(15)} = 6.329$, $R^2 = 0.727$, $p \leq 0.0001$). **(I)** Illustration of combined recordings of myotube contraction with videomicroscopy (upper trace) and electrical activity with the loose patch-technique (lower trace).

Fig. 2. Characterization of spontaneous activity of motoneuron and myotube in co-culture. **(A)** The presence of neurons in myotube culture increases the number of contracting myotubes (3.7 ± 1.3 contracting myotubes per well, $n = 4$ independent cultures, to 7.7 ± 0.5 contracting myotubes per well, $n = 4$ independent co-cultures (Mann Whitney test, $U_{(10,26)} = 0$, $p \leq 0.05$). **(B)** Confocal image of a NMJ obtained with immunostaining of motoneuron (GFP, green) contacting acetylcholine receptors (αBTX, red) expressed on a myotube (MHC, purple). **(C)** Staining of a NMJ expressing the post-synaptic marker, Rapsyn, facing the nicotinic receptors (αBTX) and the pre-synaptic neuronal marker VAChT. **(D)** Representative phase contrast image of 8 DIV neuron-myotube live co-culture. **(E)** corresponding fluorescent image of the co-culture showing the GFP-positive *Hb9::GFP* motoneurons. **(F)** Addition of neurons to myotube culture does not modify the contraction frequency (two-tailed *t* test, $t_{(43)} = 0.1708$,

$F_{(26,7)}$ = 2.5777, $p \geq 0.05$). **(G)** Addition of myotubes increases the spontaneous activity of motoneurons (from 0.5 ± 0.1 Hz, n = 22 to 1.5 ± 0.3 Hz, n = 29); (two-tailed t test, $t_{(49)}$ = 2.323, $F_{(28,21)}$ = 10.94, R^2 = 0.099, $p \leq 0.05$, from 3 WT co-cultures).

Fig. 3. $SOD1^{G93A}$ myotubes co-cultured with WT motoneurons have a decreased contraction frequency**.** **(A)** Overexpression of $SOD1^{G93A}$ in myotubes significantly decreases the contraction frequency measured using electrical spikes (1.7 ± 0.2 Hz, n = 27 and 0.9 ± 0.1 Hz, n = 34, for WT and mutant myotubes, respectively (two-tailed t test, $t_{(59)}$ = 2.952, R^2 = 0.1287, $p \leq 0.01$; $F_{(33, 26)}$ = 2.177, $p \leq 0.05$;). **(B)** Combining videomicroscopy with loose patch clamp for contraction and electrical activity recordings shows synchronization between the two activities. **(C)** Mutant myotubes retain the synchronization between contraction and electrical spike. **(D)** Mutant myotubes do not modify the frequency of Hb9::GFP motoneuron spontaneous activity (two-tailed t test, $t_{(47)}$ = 0.403, $p \geq 0.05$; $F_{(28,19)}$ = 1.611, $p \geq 0.05$).

Fig. 4. $SOD1^{G93A}$ decreases the expression of the slow myosin heavy chain isoform in myotubes. **(A)** Phase contrast image of cultured myoblasts; **(B)** phase contrast image of myotubes after 7 days in differentiation medium. **(C)** Quantitative RT-PCR of *Pax7* shows decreased expression in WT and mutant myotubes compared with myoblasts (Mann-Whitney test, $U_{(4,4)}$ = 0, $p \leq 0.05$ and $U_{(.5, 5)}$ = 0, $p \leq 0.01$, for WT and $SOD1^{G93A}$, respectively. **(D)** *Ckm* expression significantly increases in both WT and mutated myotubes (Mann-Whitney test, $U_{(4, 4)}$ = 0, $p \leq 0.05$, for WT and $SOD1^{G93A}$, respectively. **(E-I)** Quantitative RT-PCR of myosin heavy chain isoforms expressed in skeletal muscle. All isoforms are expressed, except *Mhy1*. (Mann-Whitney test: *Mhy3*: $U_{(4,4)}$ = 4, $p \geq 0.05$, for WT and $SOD1^{G93A}$, respectively; *Myh8*: $U_{(4,4)}$ = 0, $p \leq 0.05$, for WT and $SOD1^{G93A}$, respectively; *Myh2*: $U_{(4,4)}$ = 4, $p \geq 0.05$, for WT and $SOD1^{G93A}$, respectively; *Myh4*: $U_{(4,4)}$ = 0, $p \leq 0.05$, for WT and $SOD1^{G93A}$, respectively; *Myh7*: $U_{(5,5)}$ = 11, $p \geq 0.05$, and $U_{(6,6)}$ = 3, $p \leq 0.05$, for WT and $SOD1^{G93A}$, respectively).

Fig. 5. Expression of $SOD1^{G93A}$ in motoneuron reduced glutamate-driven contraction of mutant myotubes. **(A, B)** In the presence of WT motoneurons, CNQX inhibited most contractions of WT and $SOD1^{G93A}$ myotubes. **(C, D)** Expression of $SOD1^{G93A}$ in motoneurons drastically decreases the number of $SOD1^{G93A}$ and WT myotubes responding to CNQX inhibition. **(E)** The percentage of myotubes contractions inhibited by CNQX is 89 %, 78 %, 22 % and 11 % in WT co-cultures (WT/WT), in mixed mutant myotubes/WT motoneurons ($SOD1^{G93A}$/WT), mutant co-culture ($SOD1^{G93A}$/$SOD1^{G93A}$) and WT myotubes/mutant motoneurons (WT/ $SOD1^{G93A}$), respectively (WT/WT vs $SOD1^{G93A}$/WT: X^2, df = 9.899, 3, $p \geq 0.05$; WT/WT vs $SOD1^{G93A}$/$SOD1^{G93A}$: X^2, df = 9.899, 3, $p \leq 0.05$; WT/WT vs WT/ $SOD1^{G93A}$: X^2, df = 10.89, 3; $p \leq 0.05$; $SOD1^{G93A}$/$SOD1^{G93A}$ vs WT/ $SOD1^{G93A}$: X^2, df = 0.194, 3, $p \geq 0.05$).

Table

TABLE

Table 1. **Primers**. Name, sequence, amplicon length (Al) and melting point (Tm) of primers used for qRT-PCR are listed below.

Target genes	Sequences	Al	Tm
Pax7 (*paired box 7*)	F: TTCGATTAGCCGAGTGCTCA R: GATGCCATCGATGCTGTGTT	112	59
Ckm (*muscle creatine kinase*)	F: ACTACAAGCCTCAGGAGGAGTA R: TGGCCATGTGATTGTTGTGC	57	59
Myh1 *(adult Myosin Heavy Chain IIx)*	F: TTCAAGTTTGGACCCACGGT R: AGTGAGAGAGCCTGCCTTTA	54	59
Myh2 *(adult Myosin Heavy Chain IIa)*	F: TCCAAGTTCCGCAAGATCCA R: GCGCATGACCAAAGGTTTCA	193	59
Myh3 (embryonic Myosin Heavy Chain)	F: TGTTGAGATTGCAGGATCTGG R: TGCTGGGCTTTCCTGAACTT	121	59
Myh4 *(adult Myosin Heavy Chain IIb)*	F: TTCCGTAAGATCCAGCACGA R: TCCTGTCACCTCTCAACAGA	151	58
Myh7 *(adult Myosin Heavy Chain-beta)*	F: TGAGCATTCTCCTGCTGTTTC R: TGAGCCTTGGATTCTCAAACG	138	58
Myh8 (neonatal Myosin Heavy Chain)	F: ACAATCCAATGCCAACCTGG R: TCCTTCCTCTGCAAGATGTGT	156	9
Polr2j *(*polymerase (RNA) II polypeptide *J)*	F: ACCACACTCTGGGGAACATC R: CTCGCTGATGAGGTCTGTGA	160	59

Click here to access/download

Supplementary Material - Video(s)

movie 1.mp4